

# Heavy Right-Handed Neutrinos and Dark Matter in the $\nu$ CMSSM

Kenji Kadota<sup>1</sup> and Keith A. Olive<sup>2</sup>

<sup>1</sup> *Michigan Center for Theoretical Physics, University of Michigan, Ann Arbor, MI 48109*

<sup>2</sup> *William I. Fine Theoretical Physics Institute, University of Minnesota, Minneapolis, MN 55455*

February 15, 2019

## Abstract

We perform a systematic study of the effects of the type-I seesaw mechanism on the dark matter abundance in the constrained supersymmetric standard model (CMSSM) which includes three right-handed neutrinos (the  $\nu$ CMSSM). For large values of  $m_0, m_{1/2}$ , we exploit the effects of large neutrino Yukawa couplings on the renormalization group (RG) evolution of the up-type Higgs. In particular, we show that the focus point scale can greatly exceed the electroweak scale resulting in the absence of a focus point region for which the relic density of neutralinos is within the range determined by WMAP. We also discuss the effects of the right-handed neutrinos on the so-called funnel region, where the relic density is controlled by s-channel annihilations through a heavy Higgs. For small values of  $m_0, m_{1/2}$ , we discuss the possibility of sneutrino coannihilation regions with an emphasis on the suppression of the left-handed slepton doublet masses due to the neutrino Yukawa coupling. We consider two types of toy models consistent with either the normal or inverted hierarchy of neutrino masses.

## 1 Introduction

The seesaw mechanism offers a compelling explanation for the tiny masses of the left-handed neutrinos by introducing heavy gauge-singlet right-handed neutrinos which can alleviate the fine-tunings of the neutrino Yukawa couplings [1]. If the right-handed neutrino masses are close to the grand unification (GUT) scale, one typically finds neutrino Yukawa couplings of order unity. These heavy degrees of freedom may also influence such effects as lepton flavor violation [2–10] and the mass/coupling spectrum due to changes in the RG (renormalization group) evolution [11–18]. In this letter, we implement the seesaw mechanism in the context of the constrained minimal supersymmetric model (CMSSM) by adding three right-handed neutrinos  $N_i$ . We study the consequences of the near-GUT-scale right-handed neutrinos in such a model (hereafter called the  $\nu$ CMSSM) on the thermal

dark matter relic abundance which is calculated around the electroweak scale. The effects of the seesaw mechanisms on the dark matter abundance has been studied for several GUT and seesaw schemes [19–24] indicating signatures different from those in conventional CMSSM scenarios [25–32], such as the sneutrino coannihilation regions [18].

Here, we present a systematic study of the effects of a general type-I seesaw without any additional constraints from a specific GUT model which may require Yukawa coupling unification. We show in detail the behavior of two of the standard CMSSM regions where the WMAP relic density [33] is achieved, namely the funnel region, where the mass of the lightest supersymmetric particle (LSP), the neutralino, is roughly half the mass of the pseudo-scalar Higgs boson [25, 27], and the focus point region which borders the region where radiative electroweak symmetry breaking is no longer possible [28, 29, 32]. In the case of the latter, the behavior of the Higgs mass drastically changes in the  $\nu$ CMSSM because of the change in the focus point scale from the RG evolution of  $m_{H_u}^2$ . As we will see, the focus point region can even completely disappear once the energy scale of the focus point is sufficiently greater than the weak scale. As a result the WMAP strip associated with the focus point can cease to exist once the right-handed neutrino mass scale,  $M_N$ , is sufficiently large. The funnel region is also affected (though not as dramatically) as the pseudo-scalar mass is also affected by the choice of  $M_N$ .

We also detail changes in the stau coannihilation region which occurs in the CMSSM near the line of degeneracy between the neutralino and lighter stau masses. As we have shown previously [18], the introduction of a right handed neutrino can affect the running of the left-handed sleptons so that they become lighter than the more common next-to-LSP, the predominantly right-handed stau. This has the effect that the sneutrino may well become the NLSP. Here, we also extend that work to include the effects of all three right-handed neutrino states.

We review the essential features of the  $\nu$ CMSSM in §2. In §3, we consider the effect of the right-handed neutrinos on the location of the focus point regions in the  $\nu$ CMSSM. We preform an analogous analysis for the Higgs funnel regions in §4. The sneutrino coannihilation regions with small  $m_0, m_{1/2}$  are studied in §5, followed by the conclusions in §6.

## 2 $\nu$ CMSSM

For simplicity, we do not consider flavor mixings in the neutrino sector, and as such, in the basis where the heavy right-handed neutrino mass matrix is diagonal<sup>1</sup> our  $\nu$ CMSSM superpotential can be written as

$$W = W_{CMSSM} + y_{N_i} N_i^c L_i H_u + \frac{1}{2} M_{N_i} N_i^c N_i^c. \quad (1)$$

We assume that all soft SUSY breaking parameters including the soft SUSY breaking sneutrino masses,  $m_{N_i}$ , are universal at the GUT scale with value  $m_0$ . In addition, we also assume the SUSY breaking trilinear couplings including  $A_{N_i}$  are universal at the GUT scale. As in the CMSSM,

---

<sup>1</sup>We can always make the right-handed neutrino mass and lepton Yukawa coupling matrices diagonal by unitary transformations of  $N^c, L$  and  $E^c$ . The diagonal form of the neutrino Yukawa coupling matrix in such a basis is the simplification we make here.

we take universal gaugino masses. Then, in addition to the conventional CMSSM parameter set  $m_0, m_{1/2}, A_0, \tan \beta, \text{sgn}(\mu)$ , the  $\nu$ CMSSM has the following additional parameters

$$M_{N_1}(Q_{GUT}), M_{N_2}(Q_{GUT}), M_{N_3}(Q_{GUT}), m_{\nu_1}(Q_{m_Z}), m_{\nu_2}(Q_{m_Z}), m_{\nu_3}(Q_{m_Z}), \quad (2)$$

where the heavy right-handed neutrino masses  $M_{N_i}$  are specified at the GUT scale  $Q_{GUT}$ , while the light left-handed neutrino masses are specified at the weak scale,  $Q_{m_Z}$ . These boundary conditions are sufficient to determine the neutrino Yukawa couplings  $y_{N_i}$  as well. In this analysis, we restrict the right-handed neutrino masses to lie below the GUT scale  $M_{N_i} < Q_{GUT}$ . We evolve the full two-loop renormalization group equations (RGEs) in the  $\nu$ CMSSM. Each of the right-handed neutrinos decouples at  $M_{N_i}$  which itself runs from the GUT scale to  $M_{N_i}$ . Below the energy scale  $M_{N_i}$ ,  $N_i$  is integrated out and the effective Lagrangian includes the residual higher order operators suppressed by  $M_{N_i}$ . Because we are interested in the value of  $M_{N_i}$  relatively close to the GUT scale, those non-renormalizable operators do not affect the mass spectrum at the low energy scale other than the left-handed neutrino masses which receive a dominant contribution from the dimension five operator

$$L_5 \ni -\kappa(LH_u)(LH_u) \quad (3)$$

Hence, we keep the running of  $\kappa$  in our full two-loop RGEs and  $\kappa \langle H_u \rangle^2$  is matched to  $m_\nu(Q_{m_Z})$  by our electroweak scale boundary conditions [34, 35].

Even though our numerical analysis was performed including full two-loop RGEs, it will be useful to use the one-loop RGE expressions for a qualitative discussion. The relevant RGEs are ( $t \equiv \log Q$ )

$$\begin{aligned} \frac{d}{dt} m_{H_u}^2 &= \frac{1}{16\pi^2} \left( \text{Tr} \left[ 6(m_{H_u}^2 + \mathbf{m}_Q^2) \mathbf{y}_u^\dagger \mathbf{y}_u + 6 \mathbf{y}_u^\dagger \mathbf{m}_u^2 \mathbf{y}_u + 6 \mathbf{h}_u^\dagger \mathbf{h}_u + 2(m_{H_u}^2 + \mathbf{m}_L^2) \mathbf{y}_N^\dagger \mathbf{y}_N \right. \right. \\ &\quad \left. \left. + 2 \mathbf{y}_N^\dagger \mathbf{m}_N^2 \mathbf{y}_N + 2 \mathbf{h}_N^\dagger \mathbf{h}_N \right] - \frac{6}{5} g_1^2 M_1^2 - 6 g_2^2 M_2^2 + \frac{3}{5} g_1^2 S \right) + \dots \\ \frac{d}{dt} \mathbf{m}_L^2 &= \frac{1}{16\pi^2} \left( (2m_{H_d}^2 + \mathbf{m}_L^2) \mathbf{y}_e^\dagger \mathbf{y}_e + 2 \mathbf{y}_e^\dagger \mathbf{m}_E^2 \mathbf{y}_e + \mathbf{y}_e^\dagger \mathbf{y}_e \mathbf{m}_L^2 + 2 \mathbf{h}_e^\dagger \mathbf{h}_e + 2 \mathbf{y}_N^\dagger \mathbf{m}_N^2 \mathbf{y}_N \right. \\ &\quad \left. + \mathbf{y}_N^\dagger \mathbf{y}_N \mathbf{m}_L^2 + 2 \mathbf{h}_N^\dagger \mathbf{h}_N + (2m_{H_u}^2 + \mathbf{m}_L^2) \mathbf{y}_N^\dagger \mathbf{y}_N - \frac{6}{5} g_1^2 M_1^2 - 6 g_2^2 M_2^2 - \frac{3}{5} g_1^2 S \right) + \dots \\ \frac{d}{dt} \mathbf{y}_u &= \frac{\mathbf{y}_u}{16\pi^2} \left( \text{Tr} \left[ 3 \mathbf{y}_u \mathbf{y}_u^\dagger + \mathbf{y}_N \mathbf{y}_N^\dagger \right] + 3 \mathbf{y}_u^\dagger \mathbf{y}_u + \mathbf{y}_d^\dagger \mathbf{y}_d - \frac{13}{15} g_1^2 - 3 g_2^2 - \frac{16}{3} g_3^2 \right) + \dots \\ S &= \text{Tr}(\mathbf{m}_Q^2 + \mathbf{m}_D^2 - 2 \mathbf{m}_U^2 - \mathbf{m}_L^2 + \mathbf{m}_E^2) + m_{H_u}^2 - m_{H_d}^2 \end{aligned} \quad (4)$$

where, for the models to be discussed below,  $h_{ij} = A_{ij} y_{ij} \delta_{ij}$ . In the CMSSM as well as in the  $\nu$ CMSSM,  $S = 0$  at the GUT scale due to the universality of the soft scalar masses. Deviations from  $S = 0$  are due to the RG evolution at the two-loop level, hence,  $S$  does not play a significant role in our study. In the following sections, the RG effects of large neutrino Yukawa couplings on  $m_{H_u}^2$  are studied in the focus point and Higgs funnel regions whereas those effects on the slepton doublets  $\mathbf{m}_L^2$  are studied in the sneutrino/stau coannihilation regions.

We leave the question of flavor mixings and the CP violating phases for future work and we present here the analysis for two simple toy models to illustrate the effects of the heavy right-handed neutrinos on the thermal dark matter relic abundance. The first model includes only one right-handed neutrino in the third generation  $N_3$  consistent with a normal mass hierarchy  $m_{\nu_3} \gg m_{\nu_1} = m_{\nu_2}$ . To see the effects of the additional generations with multiple right-handed neutrinos, our second model includes two heavy right-handed neutrinos in the first two generations  $N_1, N_2$  leading to an inverted mass hierarchy spectrum  $m_{\nu_3} \ll m_{\nu_1} = m_{\nu_2}$ .

We start our discussion with the first model including only  $N_3$  and concentrate on large values of  $m_0, m_{1/2}$  in sections §3 and §4. In section §5, we go on to discuss our second model including two right-handed neutrinos in the first two generations  $N_1, N_2$  at relatively small  $m_0, m_{1/2}$  relevant for the sneutrino/stau coannihilation regions.

### 3 The focus point region

When the Higgsino mass parameter,  $\mu$ , becomes small or comparable to  $m_{1/2}$ , the lightest neutralino (which is typically the LSP) has an increasingly large Higgsino component and neutralino annihilations become dominated by  $W^+W^-$  final states through t-channel chargino exchange. The result of the enhanced annihilation cross section is a thermal neutralino relic abundance in the desired WMAP (95% CL) range [33]

$$0.0975 < \Omega_\chi h^2 < 0.1223 \quad (5)$$

in a region (large  $m_0$ ) where nominally the relic density is expected to be large. This region is close to the limit (at large  $m_0$ ) where there cease to be solutions to the Higgs potential minimization conditions corresponding to radiative electroweak symmetry breaking. In the CMSSM, the RGEs exhibit a focusing property leading to what is often referred to as the focus point or hyperbolic branch regions [28, 29, 32]. The RG trajectories of  $m_{H_u}^2 \sim -|\mu|^2$  for different values of  $m_0$  (and  $\tan\beta$ ) meet (or focus) near the weak scale [28]. The focusing of the RG trajectories of  $m_{H_u}^2$  also occurs in the  $\nu$ CMSSM, as the RGEs for the gaugino masses and trilinear  $A$  parameters remain independent of the scalar masses at the one-loop level (while those for the scalar masses depend on the scalar masses, gaugino masses and  $A$  parameters). In the  $\nu$ CMSSM, however, the focus point scale where RG trajectories meet is not necessarily found at the weak scale due to large neutrino Yukawa contributions. The RG evolutions of  $m_{H_u}$  in the CMSSM and  $\nu$ CMSSM are illustrated in Fig. 1 for different values of  $m_0$ , where the sign of  $m_{H_u}$  indicates the sign of  $m_{H_u}^2$ . We use a top mass  $m_t = 173.1$  GeV [36] and a bottom mass  $m_m(m_b)^{MS} = 4.25$  GeV in our analysis.

Before presenting the numerical results for the dark matter abundance calculations, we briefly examine the RG evolution of  $m_{H_u}^2$  to illustrate the properties of the focus point regions which yield the observed thermal relic abundance. The tree-level minimization of the Higgs potential gives

$$|\mu|^2 = \frac{m_{H_d}^2 - m_{H_u}^2 \tan^2 \beta}{\tan^2 \beta - 1} - \frac{M_Z^2}{2} \quad (6)$$

This allows one to estimate  $\mu^2 \approx -m_{H_u}^2 - \frac{1}{2}m_Z^2$  for moderate to large values of  $\tan\beta$  (we hereafter assume  $\mu > 0$  in our analysis as favored by measurements of  $b \rightarrow s\gamma$  and the anomalous magnetic

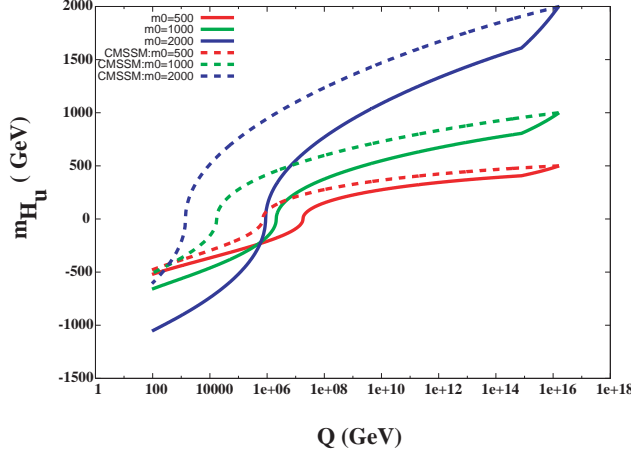


Figure 1: The RG evolutions of  $m_{H_u}$  with different values of  $m_0$  for the CMSSM (dashed) and the  $\nu$ CMSSM with  $M_{N_3} = 10^{15}$  GeV and  $m_{\nu_3} = 0.05$  eV (solid). We have set  $m_{1/2} = 300$  GeV,  $\tan \beta = 10$ ,  $A_0 = 0$ , and  $\mu > 0$ .

moment of the muon). The RGE of  $m_{H_u}^2$ , which gives us an estimate for  $\mu$  at the weak scale, is given in Eq. (4). In the CMSSM (or when  $y_N = 0$ ), we see the RG evolution of  $m_{H_u}^2$  is sensitive to the top Yukawa coupling [37, 38]. In fact, in the CMSSM, the focus point scale  $Q_{FP}$  is determined by the value of the top quark Yukawa coupling evaluated at the focus point and the (entire RG trajectories of) gauge couplings [28]. The focus point scale of  $m_{H_u}^2$  in the CMSSM turns out to be the weak scale for the measured value of top quark mass with a small dependence on moderate to large values of  $\tan \beta$  (this can be inferred from the top Yukawa coupling  $y_t \propto 1/\sin \beta \propto \text{const} + \mathcal{O}(\tan^{-2} \beta)$ ). This behavior is seen in Fig. 1 which shows the CMSSM running of  $m_{H_u}^2$  for three values of  $m_0$ . As one can clearly see, the three dashed curves corresponding to the CMSSM focus at a weak scale value for  $Q$ .

In the  $\nu$ CMSSM, the effects of the neutrino Yukawa couplings on the RGEs of  $m_{H_u}^2$  and  $y_t$  can be significant as seen in Eq. (4), so that the focus point scale of  $m_{H_u}^2$  can well exceed the weak scale. This is seen in Fig. 1 which shows the three solid curves of the  $\nu$ CMSSM focusing at the scale  $\sim 10^6$  GeV where  $y_{N_3}(Q_{GUT}) \sim 2$ . Consequently, and contrary to CMSSM, the insensitivity of  $m_{H_u}^2$  evaluated at the weak scale to  $m_0$  and  $\tan \beta$  does not necessarily hold in the  $\nu$ CMSSM.<sup>2</sup> The positions and existence of the focus point regions (at large  $m_0$  where the relic density is sufficiently small) change due to this shift in the focus point scale. When the focus point scale is below the energy scale relevant for the neutralino annihilations at which  $\mu$  is evaluated, we can decrease  $\mu \sim \sqrt{-m_{H_u}^2}$  by choosing a larger value for  $m_0$  (see CMSSM curves in Fig. 1). Recall that at small  $\mu$ , neutralino annihilation is dominated by the Higgsino component and can yield an acceptable

<sup>2</sup>Once the heavy right-handed neutrino is integrated out at  $Q = M_N$ , the analytical estimation of the focus point analogous to CMSSM can be applied to the  $\nu$ CMSSM for  $Q \leq M_N$  with non-universal scalar mass values at  $Q = M_N$ . Hence, as in the case of the CMSSM with non-universal boundary conditions, the focus point can still be found at the weak scale in the  $\nu$ CMSSM if one can tune the model parameters to realize the particular ratios of those scalar mass values at  $Q = M_N$  [28].

relic density. As one can also see from Fig. 1, when the focus point scale becomes large (as depicted in the figure for the  $\nu$ CMSSM), the weak scale value of  $m_{H_u}^2$  becomes sensitive to  $m_0$  and is driven to large negative values when  $m_0$  is large. In this case an increase of  $m_0$  (with other parameters fixed) increases  $\mu$  and the Higgsino component of the LSP is diminished and no region of suitable relic density can be found.

We also note that, for a given value of  $m_0$ , the value of  $m_{H_u}(Q)$  is smaller in the  $\nu$ CMSSM than in the CMSSM, as can be inferred from the form of RGE of  $m_{H_u}^2$  in Eq. (4) due to the additional terms involving  $y_N^2$ . The behavior of these mass parameters is also illustrated in Fig. 2 where we also show the shift/disappearance of the boundary where radiative electroweak symmetry is no longer possible. Inside the (pink) shaded region, the Higgs potential minimization conditions yield  $\mu^2 < 0$ . Along the boundary of that region  $\mu = 0$ , and close to the boundary, we show a contour of constant  $\mu = 200$  GeV. Almost coinciding with that contour is the very thin WMAP focus point region (shaded turquoise) where the relic density lies in the range given in Eq. (5). Also shown are contours of constant  $\mu$  at 200 GeV intervals. As one can see, as  $M_{N_3}$  is increased, the focus point region shifts to increasing  $m_0$  and is absent at  $M_{N_3} \sim 10^{14}$  GeV (which corresponds to  $y_{N_3}(Q_{GUT}) \sim 0.6$ ) at which point there is no longer any sensitivity of the value of  $\mu$  to  $m_0$ . This corresponds to the coincidence of the focus point scale with the scale at which  $\mu$  is evaluated. In this figure, we have fixed  $m_{1/2} = 300$  GeV,  $\tan \beta = 10$  and  $A_0 = 0$ . For  $M_{N_3} \lesssim 10^{14}$  GeV, the focus point energy scale,  $Q_{FP}$  is low and increasing  $m_0$  helps making  $m_{H_u}^2$  less negative which reduces  $\mu$  allowing for the presence of the focus point region. For larger  $M_{N_3}$ , the opposite behavior occurs and increasing  $m_0$  increases  $\mu$ .

Fig. 2 also shows the region where the two-loop contributions become large. To the right of the vertical dashed line at  $M_{N_3} \sim 2 \times 10^{15}$  GeV,  $y_{N_3}^2/16\pi^2 > 1/10$  (where the dominant two loop contribution is roughly 1/4 of the 1-loop contribution). At larger values of  $M_{N_3}$ , our perturbative calculation results could become unreliable [4, 7, 39]. To the left of this line, we see that  $\mu$  increases with  $M_{N_3}$  for fixed  $m_0$ . Finally, in the region below the (red) dot-dashed curve,  $m_h < 114.4$  GeV and fails the LEP limit [40] (modulo the uncertainty in the calculation of  $m_h$  for which FeynHiggs [41] was used here).

Our qualitative discussion so far can be summarized in Fig. 3 which shows the  $(m_0, m_{1/2})$  plane for  $\tan \beta = 10$  and  $A_0 = 0$ . In the lower right corner of the figure, the dark (red) shaded region corresponds to parameters for which the LSP is the charged partner of the tau lepton and as such is excluded. Running along this region is the so-called WMAP co-annihilation strip, where co-annihilations between neutralinos and staus are largely responsible for obtaining the WMAP relic density. This area (as in the previous figure) is shaded turquoise. In the lower left corner of the figure, the small dark (green) shaded region is excluded as the supersymmetric contributions to  $b \rightarrow s\gamma$  disagree with the experimental determination [42], while the light pink shaded region is favored by the measurement of the muon anomalous magnetic moment at the 2- $\sigma$  level [43]. The red dot-dashed contour corresponds to a Higgs mass of 114.4 GeV. At lower  $m_{1/2}$ , the Higgs boson would be lighter, which is excluded by its non-observation at LEP [40]. We also plot a black dashed contour for  $m_{\chi^\pm} = 104$  GeV, the region at lower  $m_{1/2}$  also being excluded by LEP. These contours are shown for four choices of  $M_{N_3}$  as labelled. Note that the stau co-annihilation strip is barely sensitive to the choices of  $M_{N_3}$  made here as are other quantities at low  $m_0$ . This is reasonable

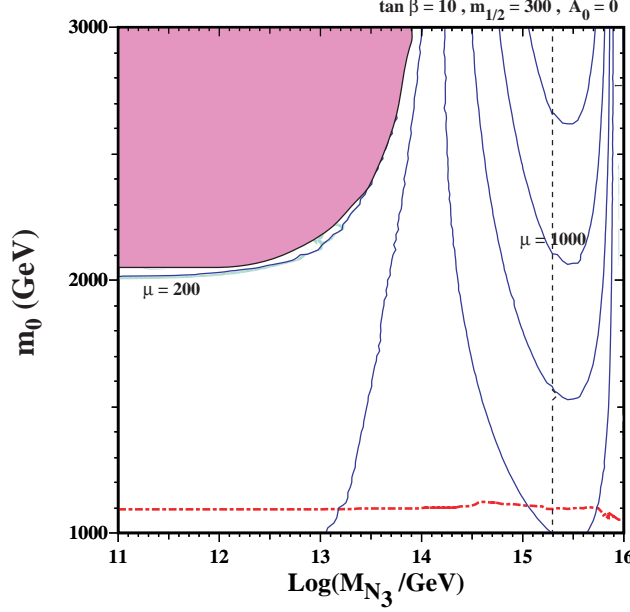


Figure 2: The  $(m_0, M_{N_3})$  plane for fixed  $m_{1/2} = 300$  GeV,  $\tan \beta = 10$ ,  $A_0 = 0$ , and  $m_{\nu_3} = 0.05$  eV. The (pink) shaded region shows the portion of parameter space where the radiative electroweak symmetry breaking conditions can not be satisfied. The focus point region (turquoise) compatible with Eq. (5) runs along this boundary nearly coinciding with the contour for  $\mu = 200$  GeV. Other contours of constant  $\mu$  are also shown. The (red) dot-dashed curve shows the contour of  $m_h = 114.4$  GeV. Below this curve, the Higgs mass is below the LEP limit. To the right of the vertical dashed line,  $y_{N_3}^2/16\pi^2 > 1/10$  and our perturbative expansion becomes suspect.

because the terms involving a neutrino Yukawa coupling in the RGE of the slepton doublets can become large when the scalar masses or trilinear A terms are large as seen in Eq. (4). Because the gaugino masses and the right-handed stau are not affected by a neutrino Yukawa coupling at the one loop-level, the ratio of the stau and gaugino mass would not be affected significantly by the right-handed neutrino when  $m_0$  and  $A$  are small.

In the upper left corner of Fig. 3, we see the (pink) shaded region where there is no radiative electroweak symmetry breaking. Along the boundary of this region, we find the focus point strip where again the relic density of neutralinos is within the WMAP range. The shaded region corresponds to the standard CMSSM model or equivalently the  $\nu$ CMSSM with  $M_{N_3} = Q_{\text{GUT}} \simeq 2 \times 10^{16}$  GeV. Within the shaded region, we also show how the region of no radiative electroweak symmetry breaking recedes to higher  $m_0$  for values of  $M_{N_3} < Q_{\text{GUT}}$ . The boundary in each case is shown labelled by the chosen value of  $M_{N_3}$ . The WMAP focus point strip would run along each boundary. Note that for very low  $M_{N_3}$  ( $\sim 2 \times 10^{12}$  GeV), we effectively recover the CMSSM as the neutrino Yukawa couplings are too small to have any effect on RGEs. As  $M_{N_3}$  is increased, we see the disappearance of the focus point region as discussed above.

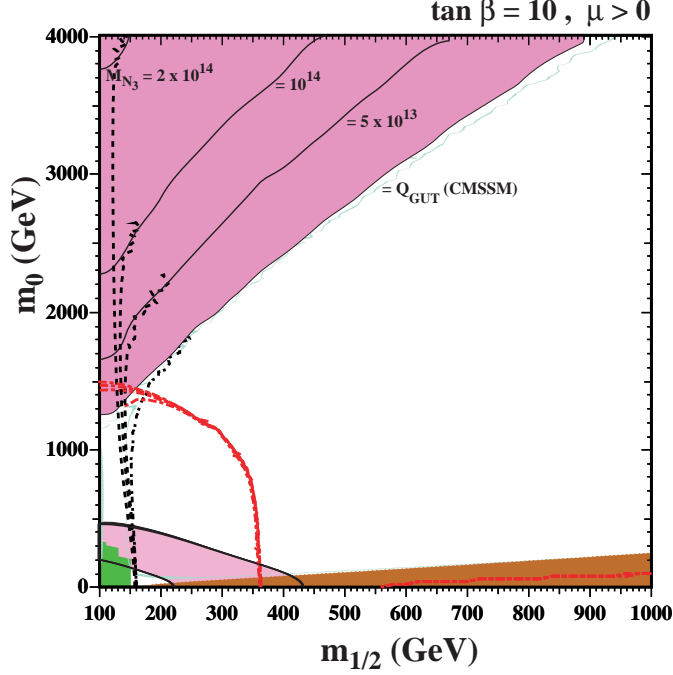


Figure 3: The  $(m_0, m_{1/2})$  plane for  $\tan \beta = 10$ ,  $A_0 = 0$ ,  $m_{\nu_3} = 0.05\text{eV}$ , and four choices of  $M_{N_3}$ . The region labelled  $Q_{\text{GUT}}$  corresponds to the CMSSM. The black solid lines represent the boundaries of the regions above which (i.e. for bigger  $m_0$ ) there is no electroweak symmetry breaking and  $\mu^2 < 0$ . Contours and shaded regions are described in the text.

## 4 Higgs funnel region

Another efficient neutralino annihilation process which results in the requisite thermal relic density is through the s-channel Higgs (A and H) resonances and is possible at large  $\tan \beta$ . The dominant contributions are through the pseudo-scalar A which is CP odd and can couple to initial s-wave states (while the couplings through the CP-even H suffer from p-wave suppressions due to the small velocity of the neutralinos), with the dominant final states  $b\bar{b}$  whose coupling is enhanced by a factor  $\propto m_b \tan \beta$ . At large  $\tan \beta$ , the resonances become broad enough (typically  $10 \sim 50\text{GeV}$ ) so that sufficient neutralino annihilations can occur even if  $m_\chi$  is several partial widths away from the exact resonance region  $2m_\chi = m_A$ . The change in the RG evolution of  $m_{H_u}^2$  in the  $\nu\text{CMSSM}$  also affects the A-pole funnel regions. This can be understood from the tree-level Higgs potential which gives

$$m_A^2 = m_{H_d}^2 + m_{H_u}^2 + 2|\mu|^2 \quad (7)$$

which, for moderate to large  $\tan \beta$ , becomes

$$m_A^2 \approx m_{H_d}^2 - m_{H_u}^2 - m_Z^2. \quad (8)$$



For fixed  $m_0$ , and noting that the gaugino mass RGEs include  $y_N$  at the two-loop level, we would expect the Higgs funnel regions to move towards larger  $m_{1/2}$  for larger  $y_N$ . This is because  $y_N$  increases  $m_A$  by making  $m_{H_u}^2$  more negative and hence requires larger  $m_{1/2}$  in order to satisfy  $2m_\chi \sim m_A$ . For  $m_{1/2}$  fixed, the increase in  $m_A$  from an increase in  $y_N$  must be compensated by a decrease in  $m_0$ . This is because a decrease in  $m_0$  can change  $m_{H_d}^2$  (which is affected by  $y_N$  at the two-loop level) to cancel the change in  $m_{H_u}^2$  and can also suppress the terms in the RGE which involve the products of  $y_N^2$  and scalar mass squared. These effects are summarized in Figs. 4 and 5. Fig. 4 shows the contours of  $m_A/2m_\chi$  in the  $(m_0, M_{N_3})$  plane. Here, we can see the broad Higgs funnel region extending between the  $m_A/2m_\chi = 1$  and 1.1 contours. The Higgs resonance is so efficient such that the WMAP strips typically show up slightly off the exact resonance  $m_A/2m_\chi = 1$  contour line. In the dark (red) shaded region at lower  $m_0$ , the lightest stau is the LSP and hence this region is excluded. Between this region and the WMAP strip, the relic density is lower than the WMAP range.

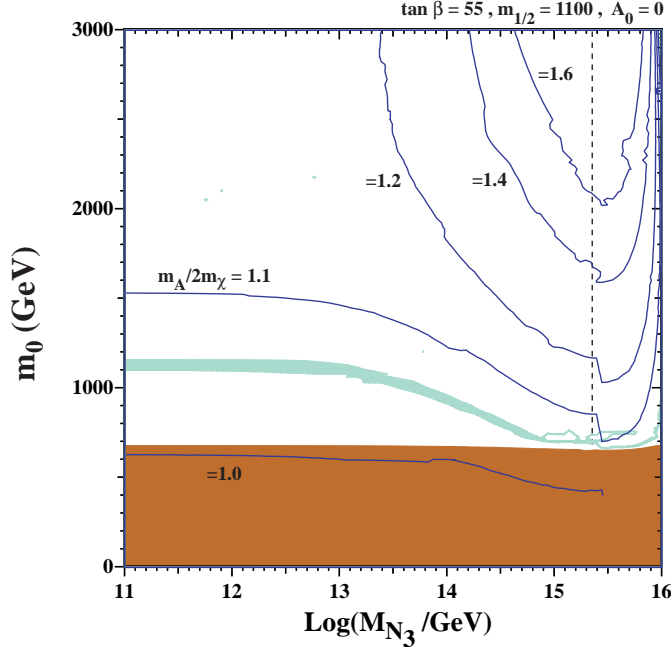


Figure 4: The  $(m_0, M_{N_3})$  plane for fixed  $m_{1/2} = 1100$  GeV,  $\tan \beta = 55$ ,  $A_0 = 0$ , and  $m_{\nu_3} = 0.05$  eV. The funnel region (turquoise) compatible with Eq. (5) runs almost horizontally around  $m_0 \simeq 1100$  GeV. Contours of constant  $m_A/2m_\chi$  are also shown. To the right of the vertical dashed line,  $y_{N_3}^2/16\pi^2 > 1/10$  and our perturbative expansion becomes suspect.

Fig. 5 shows the  $(m_0, m_{1/2})$  plane at  $\tan \beta = 55$  for which the funnel region is clearly visible. As in Fig. 3, we show the position of the Higgs and chargino mass contours at the LEP limit. Also shown are the shaded regions excluded by a charged stau LSP and  $b \rightarrow s\gamma$  as well as the shaded region preferred by  $g_\mu - 2$ . The shaded region in the upper left again corresponds to the region with no radiative electroweak symmetry breaking in the CMSSM. The shaded region labelled

CMSSM, corresponds to the funnel region where the relic density agrees with the WMAP range. The remaining funnel-like shaded regions correspond to the shift in the funnel in the  $\nu$ CMSSM for different values of  $M_{N_3} = 2 \times 10^{13}$  GeV,  $5 \times 10^{13}$  GeV and  $10^{14}$  GeV. Fig. 4 corresponded to the choice  $m_{1/2} = 1100$  GeV, and as one can see for values of  $m_0$  above the line of neutralino-stau degeneracy and below the WMAP funnel, s-channel neutralino annihilations via the heavy Higgs are so strong near  $m_{\tilde{\tau}} \sim m_{\chi}$  that the relic density is pushed to values far below the WMAP range. As such, for this value of  $m_{1/2}$  there is no WMAP stau coannihilation region.

As the neutrino Yukawa coupling becomes larger, the funnel regions move down towards the stau coannihilation regions. Also note that the larger values of  $\mu$  obtained through the effects of the neutrino Yukawa couplings increase the left-right mixings in the stau mass matrix, especially for large  $\tan\beta$ , due to the off-diagonal term  $-m_{\tau}(\mu \tan\beta + A_{\tau})$ . The neutrino Yukawa couplings can also increase the left-handed component in the lighter slepton mass eigenstate by suppressing the left-handed slepton mass as discussed in §5.2.

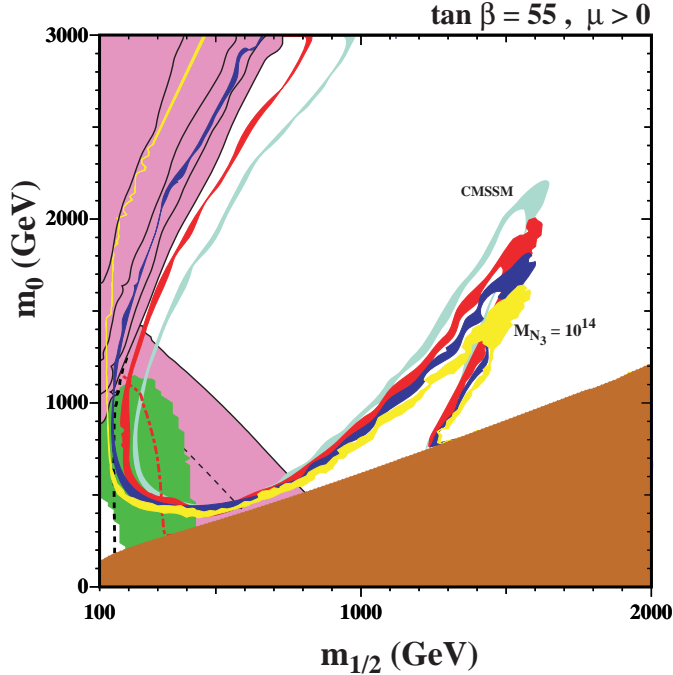


Figure 5: As in Fig. 3, the funnel regions for the CMSSM and for different values of  $M_{N_3} = 2 \times 10^{13}, 5 \times 10^{13}, 10^{14}$  GeV in the  $\nu$ CMSSM.

The focus point strip is also visible in Fig. 5. For the case of the CMSSM, in the area between the focus point strip and the shaded region corresponding to  $\mu^2 < 0$ , the lightest neutralino acquires a significant Higgsino component and the relic density is below the WMAP range. As discussed in the previous section, as  $M_{N_3}$  is increased, the focus point strips move to larger values of  $m_0$ . The black solid lines to the left of each colored strip corresponds to the edge of the region where radiative electroweak symmetry breaking is lost.

## 5 Effects from the first two generation right-handed neutrinos

We have so far discussed the effects of only one heavy right-handed neutrino in the third generation exemplifying a normal hierarchy scenario  $m_{\nu 3} \gg m_{\nu 1} \approx m_{\nu 2}$ . That is we have implicitly assumed that the Yukawa couplings for the first two generation neutrinos are small and do not affect the particle spectrum. We next consider the effects of multiple right-handed neutrinos in other generations for comparison. We then go on to explore how the parameter space at relatively low  $m_{1/2}$  and  $m_0$  is affected by the seesaw mechanism, with an emphasis on the emergence of sneutrino coannihilation regions.

### 5.1 Focus and Higgs funnel regions

We now consider a model which includes  $N_1$  and  $N_2$  with equal masses,  $M_{N_1} = M_{N_2}$ , corresponding to an inverted mass hierarchy  $m_{\nu 3} \ll m_{\nu 1} = m_{\nu 2}$ . Even though this toy model is not complete in that we ignore the neutrino mixings for simplicity, it does illustrate the features of the  $e$  and  $\mu$  right-handed neutrinos which are distinct from those of the  $\tau$  right-handed neutrino and those of the CMSSM. We save a more complete analysis including all three neutrinos and mixings for a future publication.

The effects of  $N_1$  and  $N_2$  on the Higgs masses are qualitatively analogous to those of  $N_3$  because the neutrino Yukawa coupling term,  $y_{ij} N_i L_j H_u$ , ( $y_{ij}$  is diagonal in this example) which gives the key interactions between  $N_i$  and the Higgs bosons has a common form for each generation. Thus we expect similar effects on the RG evolution of  $m_{H_u}^2$  (or  $\mu$ ) as discussed above. The effect of making  $m_{H_u}^2$  even more negative is, however, bigger now because there are contributions from both first and second generations, and hence the shift and disappearance of the focus point and funnel regions are more prominent quantitatively. As one can see from Fig. 6, the edge of the region with no electroweak symmetry breaking at large  $m_0$  is shifted down in  $M_{N_1}$  by a factor of two relative to where it was in Fig. 2 for  $N_3$ . The sensitivity of  $\mu$  on  $M_{N_1}, M_{N_2}$  is also shown in Fig. 6.

### 5.2 Sneutrino coannihilation regions

Our final consideration is the sneutrino coannihilation region at relatively small  $m_0$  and  $m_{1/2}$ . Here, the qualitative interpretation of the parameter space compatible with the observed dark matter abundance can differ significantly between the two toy models discussed in this paper. Sneutrino coannihilation regions where the sneutrino is the NLSP with a neutralino LSP are not realized in the CMSSM because the right-handed species are usually lighter than the corresponding left-handed slepton doublets. This is because the SU(2) gauge coupling terms in the RGEs tend to push the masses of slepton doublets up over their right-handed counter parts when universal boundary conditions at the high energy scale are chosen as in the CMSSM. In the  $\nu$ CMSSM, however, the neutrino Yukawa coupling which involves the left-handed SU(2) doublet  $y_N N L H_u$  can push the left-handed slepton doublet mass down while running from  $Q = Q_{GUT}$  down to  $Q = M_N$ , enabling

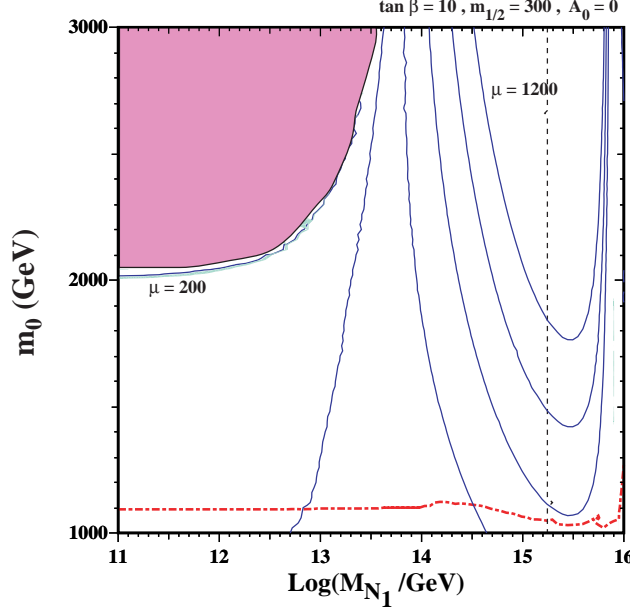


Figure 6: As in Fig. 2, the  $(m_0, M_{N_1})$  plane for fixed  $m_{1/2} = 300$  GeV,  $\tan\beta = 10$ ,  $A_0 = 0$ , and  $m_{\nu_1} = m_{\nu_2} = 0.05$  eV. It is assumed that  $M_{N_1} = M_{N_2}$ .

the slepton doublets to be lighter than their corresponding right-handed singlets at the electroweak scale.

In the model with a single right handed neutrino ( $N_3$ ), the realization of the sneutrino coannihilation regions tends to require a large value of  $A_0$  and a moderate value of  $\tan\beta$  [18]. A small universal scalar mass is generally required to make the sneutrino light, which results in the necessity for large  $A_0$  because the effects of the neutrino Yukawa coupling show up in the RGEs in the form of a product between  $y_N$  and the sum of scalar masses and  $A_0$  as given in Eq. (4). Large  $A_0$  also helps enhance the stop loop contributions to the Higgs mass which relaxes the tight constraint from Higgs mass lower bound when  $m_{1/2}$  is small (low  $m_{1/2}$  is also preferred in order to obtain a light sneutrino by suppressing the the RG evolution of the slepton doublet due to gauge interactions). Moderate  $\tan\beta$  is preferred because at large  $\tan\beta$  the induced mixing in the stau mass matrix is too large and causes one of the stau mass eigenstates to be run below the sneutrino mass.

Fig. 7 shows the  $(m_0, m_{1/2})$  plane in the  $\nu$ CMSSM for the two types of models considered (corresponding to the normal and inverted hierarchies). As in Figs. 3 and 5, the dark (red) shaded region is excluded because the LSP is the charged partner of the stau. In the left portion of each plane, there are areas where one or more of the sparticles are tachyonic. This relatively large region is shaded pink. There is also a region which is excluded by measurements of  $b \rightarrow s\gamma$  and these (shaded green) also exclude low values of  $m_{1/2}$ . In the background of each panel, there is a light blue shaded region where the value of  $g_\mu - 2$  is in agreement with the observed discrepancy to within  $2\sigma$ . In the right panel, this region is more prominent and the area within the dashed contour satisfies the  $g_\mu - 2$  constraint within  $1\sigma$ . The dark blue shaded region in each figure is a direct

result of the  $\nu$ CMSSM and corresponds to the area where a sneutrino is the LSP. This region is also excluded [44]. Finally, there is the region where the relic density matches the WMAP determination as shown by the thin turquoise strips which track either the stau or sneutrino LSP regions. The relic density in each case is brought to an acceptable value through neutralino coannihilations with staus [45] and/or sneutrinos [46].

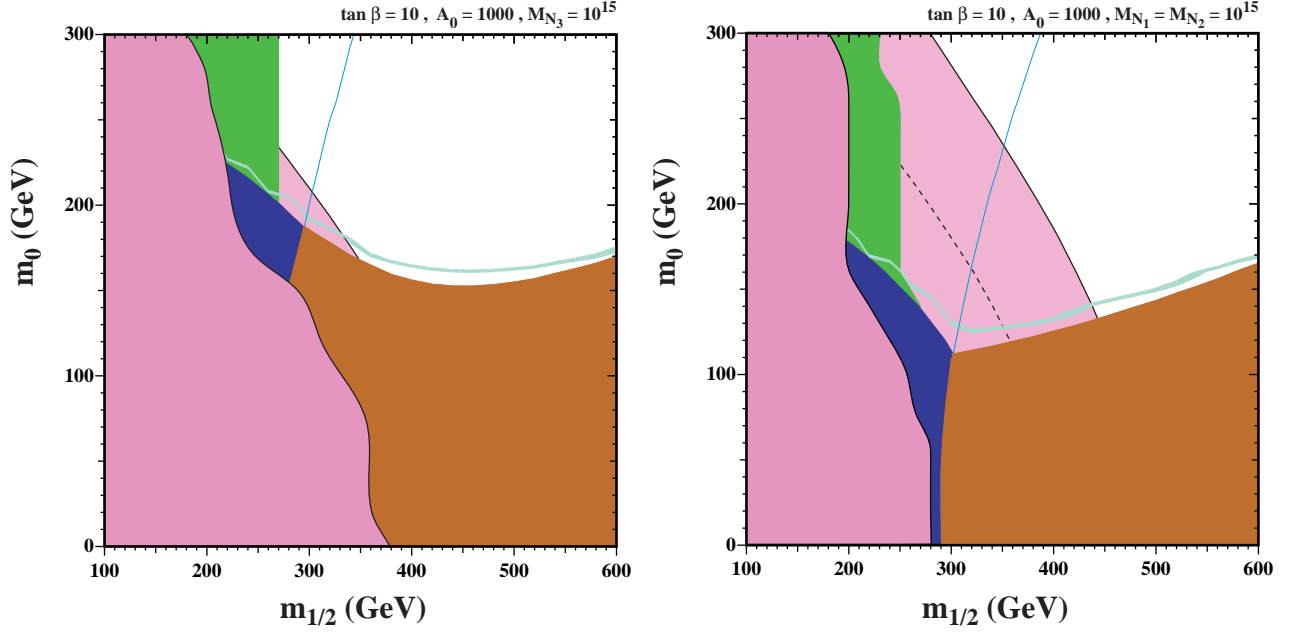


Figure 7: The  $(m_0, m_{1/2})$  plane in the  $\nu$ CMSSM. In both panels,  $\tan \beta = 10$  and  $A_0 = 1000$  GeV. In the left panel,  $M_{N_3} = 10^{15}$  GeV and corresponds to the case of a normal neutrino mass hierarchy while in the right panel,  $M_{N_1} = M_{N_2} = 10^{15}$  GeV corresponding to an inverted hierarchy. Contours and shading are described in the text.

For our normal hierarchy model shown in the left panel of Fig. 7, the stau coannihilation region is adjacent to the tau sneutrino NLSP regions (the thin blue line shows the position of the contour  $m_{\tilde{\nu}}/m_{\tilde{\tau}} = 1$ ). Analogous to the  $\tau$  sneutrino coannihilation regions,  $e/\mu$  sneutrino coannihilation regions appear in our second toy model shown in the right panel of Fig. 7. In this case, the effects of the right-handed neutrinos in reducing the left-handed slepton mass is more prominent than in the model with a normal neutrino mass hierarchy. For instance, sneutrino coannihilation regions show up for  $A_0 \gtrsim 700$  GeV for our inverted mass hierarchy toy model with  $M_{N_1} = M_{N_2} = 10^{15}$  GeV,  $m_{\nu_1} = m_{\nu_2} = 0.05$  eV, while  $A_0 \gtrsim 1000$  GeV is required for our normal mass hierarchy toy model with  $M_{N_3} = 10^{15}$  GeV,  $m_{\nu_3} = 0.05$  eV (and other parameter values are fixed as in Fig. 7). For the electron/muon sneutrino coannihilation regions, the WMAP strip transition corresponds to the abrupt change from the mostly horizontal right-handed stau NLSP region to the more vertical left-handed electron/muon sneutrino NLSP region. For the tau sneutrino NLSP, in contrast, the transition from the stau coannihilation region to the tau sneutrino coannihilation region corresponds to the smooth change of the stau chirality which is initially right-chiral dominated with an increasing

left-chiral component for smaller  $m_{1/2}$ , before it eventually shifts to the tau sneutrino NLSP region. This is expected as the left-handed slepton doublet becomes light due to a large neutrino Yukawa coupling in a region with small  $m_{1/2}$ . The tau sneutrino typically accompanies an almost degenerate left-handed stau state with their small mass splitting coming from D-term contributions, hence resulting in nearly parallel contours for  $m_{\tilde{\nu}_\tau}/m_\chi = 1$  and  $m_{\tilde{\tau}}/m_\chi = 1$  in the left panel in Fig. 7, while a more abrupt transition from the (right-handed) stau coannihilation to the (left-handed) electron/muon sneutrino coannihilation regions arises in the right panel.

## 6 Conclusion

The CMSSM has been studied extensively as a template to see the general features of a simple supersymmetric model. Given the necessity for neutrino masses, the CMSSM implicitly assumes that the additional operators relevant to neutrino masses are sufficiently small that their presence in the running of the supersymmetric particle spectrum can be ignored. In effect, from the viewpoint of the seesaw scheme, such an extension of the CMSSM assumes a relatively low value for the heavy right-handed neutrino masses. The  $\nu$ CMSSM is an extension of the CMSSM and explicitly includes three right-handed neutrinos in a general type-I seesaw setup while keeping the universal boundary conditions as in CMSSM. Here, we have studied how the dark matter abundances are affected by presence of right-handed neutrinos whose masses are close to the GUT scale. Though we ignored flavor mixing and the CP violating phase in the neutrino mass matrix, our two simple models illustrate the intriguing effects of GUT scale right-handed neutrinos. These include the change in the focus point scale, shifts in the funnel region and the realization of light left-handed slepton doublets. Clearly the GUT-scale seesaw mechanism and its effects on low-energy observables deserves further study.

This work was supported by Michigan Center for Theoretical Physics (KK), DOE grant DE-FG02-94ER-40823 and the William I. Fine Theoretical Physics Institute (KAO).

## References

- [1] P. Minkowski, Phys. Lett. B **67** (1977) 421.; M. Gell-Mann, P. Ramond, and R. Slansky, in *Supergravity*, eds. D.Z. Freedman and P. van Nieuwenhuizen, North Holland (1979); T. Yanagida, in Proceedings of the Workshop on the Unified Theory and The Baryon Number of the Universe, eds O. Sawada and S. Sugamoto. KEK79-18 (1979).
- [2] F. Borzumati and A. Masiero, Phys. Rev. Lett. **57**, 961 (1986).
- [3] J. Hisano, T. Moroi, K. Tobe and M. Yamaguchi, Phys. Rev. D **53**, 2442 (1996) [arXiv:hep-ph/9510309].
- [4] J. A. Casas, J. R. Espinosa, A. Ibarra and I. Navarro, Nucl. Phys. B **569**, 82 (2000) [arXiv:hep-ph/9905381].

- [5] S. Lavignac, I. Masina and C. A. Savoy, models,” Phys. Lett. B **520**, 269 (2001) [arXiv:hep-ph/0106245].
- [6] J. R. Ellis, J. Hisano, S. Lola and M. Raidal, Nucl. Phys. B **621**, 208 (2002) [arXiv:hep-ph/0109125].
- [7] B. A. Campbell and D. W. Maybury, JHEP **0704**, 077 (2007) [arXiv:hep-ph/0603053].
- [8] A. Dedes, H. E. Haber and J. Rosiek, JHEP **0711**, 059 (2007) [arXiv:0707.3718 [hep-ph]].
- [9] A. Ibarra and C. Simonetto, JHEP **0804**, 102 (2008) [arXiv:0802.3858 [hep-ph]].
- [10] M. Hirsch, J. W. F. Valle, W. Porod, J. C. Romao and A. Villanova del Moral, Phys. Rev. D **78**, 013006 (2008) [arXiv:0804.4072 [hep-ph]].
- [11] J. A. Casas, J. R. Espinosa, A. Ibarra and I. Navarro, Phys. Rev. D **63**, 097302 (2001) [arXiv:hep-ph/0004166].
- [12] H. Baer, C. Balazs, J. K. Mizukoshi and X. Tata, Phys. Rev. D **63**, 055011 (2001) [arXiv:hep-ph/0010068].
- [13] H. Baer, C. Balazs, M. Brhlik, P. Mercadante, X. Tata and Y. Wang, Phys. Rev. D **64**, 015002 (2001) [arXiv:hep-ph/0102156].
- [14] G. A. Blair, W. Porod and P. M. Zerwas, Eur. Phys. J. C **27**, 263 (2003) [arXiv:hep-ph/0210058].
- [15] M. R. Buckley and H. Murayama, Phys. Rev. Lett. **97**, 231801 (2006) [arXiv:hep-ph/0606088].
- [16] G. L. Kane, P. Kumar, D. E. Morrissey and M. Toharia, Phys. Rev. D **75**, 115018 (2007) [arXiv:hep-ph/0612287].
- [17] J. A. Casas, A. Ibarra and F. Jimenez-Alburquerque, JHEP **0704**, 064 (2007) [arXiv:hep-ph/0612289].
- [18] K. Kadota, K. A. Olive and L. Velasco-Sevilla, Phys. Rev. D **79**, 055018 (2009) arXiv:0902.2510 [hep-ph].
- [19] S. T. Petcov, S. Profumo, Y. Takanishi and C. E. Yaguna, Nucl. Phys. B **676**, 453 (2004) [arXiv:hep-ph/0306195].
- [20] L. Calibbi, Y. Mambrini and S. K. Vempati, JHEP **0709**, 081 (2007) [arXiv:0704.3518 [hep-ph]].
- [21] V. Barger, D. Marfatia and A. Mustafayev, Phys. Lett. B **665**, 242 (2008) [arXiv:0804.3601 [hep-ph]].
- [22] M. E. Gomez, S. Lola, P. Naranjo and J. Rodriguez-Quintero, arXiv:0901.4013 [hep-ph].

- [23] J. N. Esteves, M. Hirsch, S. Kaneko, W. Porod and J. C. Romao, arXiv:0907.5090 [hep-ph].
- [24] V. Barger, D. Marfatia, A. Mustafayev and A. Soleimani, arXiv:0908.0941 [hep-ph].
- [25] M. Drees and M. M. Nojiri, Phys. Rev. D **47** (1993) 376 [arXiv:hep-ph/9207234]; H. Baer and M. Brhlik, Phys. Rev. D **53** (1996) 597 [arXiv:hep-ph/9508321]; Phys. Rev. D **57** (1998) 567 [arXiv:hep-ph/9706509]; H. Baer, M. Brhlik, M. A. Diaz, J. Ferrandis, P. Mercadante, P. Quintana and X. Tata, Phys. Rev. D **63** (2000) 015007 [arXiv:hep-ph/0005027]; A. B. Lahanas, D. V. Nanopoulos and V. C. Spanos, Mod. Phys. Lett. A **16** (2001) 1229 [arXiv:hep-ph/0009065].
- [26] J. R. Ellis, T. Falk, K. A. Olive and M. Schmitt, Phys. Lett. B **388** (1996) 97 [arXiv:hep-ph/9607292]; Phys. Lett. B **413** (1997) 355 [arXiv:hep-ph/9705444]; J. R. Ellis, T. Falk, G. Ganis, K. A. Olive and M. Schmitt, Phys. Rev. D **58** (1998) 095002 [arXiv:hep-ph/9801445]; V. D. Barger and C. Kao, Phys. Rev. D **57** (1998) 3131 [arXiv:hep-ph/9704403]; J. R. Ellis, T. Falk, G. Ganis and K. A. Olive, Phys. Rev. D **62** (2000) 075010 [arXiv:hep-ph/0004169]; V. D. Barger and C. Kao, Phys. Lett. B **518** (2001) 117 [arXiv:hep-ph/0106189]; L. Roszkowski, R. Ruiz de Austri and T. Nihei, JHEP **0108** (2001) 024 [arXiv:hep-ph/0106334]; A. B. Lahanas and V. C. Spanos, Eur. Phys. J. C **23** (2002) 185 [arXiv:hep-ph/0106345]; A. Djouadi, M. Drees and J. L. Kneur, JHEP **0108** (2001) 055 [arXiv:hep-ph/0107316]; U. Chattopadhyay, A. Corsetti and P. Nath, Phys. Rev. D **66** (2002) 035003 [arXiv:hep-ph/0201001]; J. R. Ellis, K. A. Olive and Y. Santoso, New Jour. Phys. **4** (2002) 32 [arXiv:hep-ph/0202110]; H. Baer, C. Balazs, A. Belyaev, J. K. Mizukoshi, X. Tata and Y. Wang, JHEP **0207** (2002) 050 [arXiv:hep-ph/0205325]; R. Arnowitt and B. Dutta, arXiv:hep-ph/0211417.
- [27] J. R. Ellis, T. Falk, G. Ganis, K. A. Olive and M. Srednicki, Phys. Lett. B **510** (2001) 236 [arXiv:hep-ph/0102098].
- [28] J. L. Feng and K. T. Matchev, Phys. Rev. D **63**, 095003 (2001) [arXiv:hep-ph/0011356]; J. L. Feng, K. T. Matchev and T. Moroi, Phys. Rev. D **61**, 075005 (2000) [arXiv:hep-ph/9909334].
- [29] J. L. Feng, K. T. Matchev and F. Wilczek, Phys. Lett. B **482**, 388 (2000) [arXiv:hep-ph/0004043].
- [30] J. R. Ellis, K. A. Olive, Y. Santoso and V. C. Spanos, Phys. Lett. B **565** (2003) 176 [arXiv:hep-ph/0303043].
- [31] H. Baer and C. Balazs, JCAP **0305**, 006 (2003) [arXiv:hep-ph/0303114]; A. B. Lahanas and D. V. Nanopoulos, Phys. Lett. B **568**, 55 (2003) [arXiv:hep-ph/0303130]; U. Chattopadhyay, A. Corsetti and P. Nath, Phys. Rev. D **68**, 035005 (2003) [arXiv:hep-ph/0303201]; C. Munoz, Int. J. Mod. Phys. A **19**, 3093 (2004) [arXiv:hep-ph/0309346].



- [32] K. L. Chan, U. Chattopadhyay and P. Nath, Phys. Rev. D **58**, 096004 (1998) [arXiv:hep-ph/9710473]; J. L. Feng, K. T. Matchev and T. Moroi, Phys. Rev. Lett. **84**, 2322 (2000) [arXiv:hep-ph/9908309]; H. Baer, T. Krupovnickas and X. Tata, JHEP **0307**, 020 (2003) [arXiv:hep-ph/0305325]; G. Belanger, S. Kraml and A. Pukhov, Phys. Rev. D **72**, 015003 (2005) [arXiv:hep-ph/0502079]; H. Baer, T. Krupovnickas, S. Profumo and P. Ullio, JHEP **0510** (2005) 020 [arXiv:hep-ph/0507282].
- [33] J. Dunkley *et al.* [WMAP Collaboration], Astrophys. J. Suppl. **180**, 306 (2009) [arXiv:0803.0586 [astro-ph]].
- [34] S. Antusch and M. Ratz, JHEP **0207**, 059 (2002) [arXiv:hep-ph/0203027].
- [35] S. Antusch, J. Kersten, M. Lindner, M. Ratz and M. A. Schmidt, JHEP **0503**, 024 (2005) [arXiv:hep-ph/0501272].
- [36] [Tevatron Electroweak Working Group and CDF Collaboration and D0 Collaboration], arXiv:0803.1683 [hep-ex], arXiv:0903.2503 [hep-ex].
- [37] H. Baer, T. Krupovnickas and X. Tata, JHEP **0307**, 020 (2003) [arXiv:hep-ph/0305325].
- [38] H. Baer, A. Mustafayev, S. Profumo, A. Belyaev and X. Tata, JHEP **0507**, 065 (2005) [arXiv:hep-ph/0504001].
- [39] G. Belanger, S. Kraml and A. Pukhov, Phys. Rev. D **72**, 015003 (2005) [arXiv:hep-ph/0502079]; B. C. Allanach, S. Kraml and W. Porod, JHEP **0303**, 016 (2003) [arXiv:hep-ph/0302102].
- [40] Joint LEP 2 Supersymmetry Working Group, *Combined LEP Chargino Results, up to 208 GeV*, [http://lepsusy.web.cern.ch/lepsusy/www/inos\\_moriond01/charginos\\_pub.html](http://lepsusy.web.cern.ch/lepsusy/www/inos_moriond01/charginos_pub.html); LEP Higgs Working Group for Higgs boson searches, OPAL Collaboration, ALEPH Collaboration, DELPHI Collaboration and L3 Collaboration, Phys. Lett. B **565** (2003) 61 [arXiv:hep-ex/0306033]. *Search for neutral Higgs bosons at LEP*, paper submitted to ICHEP04, Beijing, LHWG-NOTE-2004-01, ALEPH-2004-008, DELPHI-2004-042, L3-NOTE-2820, OPAL-TN-744, [http://lephiggs.web.cern.ch/LEPHIGGS/papers/August2004\\_MSSM/index.html](http://lephiggs.web.cern.ch/LEPHIGGS/papers/August2004_MSSM/index.html).
- [41] S. Heinemeyer, W. Hollik and G. Weiglein, *Comput. Phys. Commun.* **124** (2000) 76 [arXiv:hep-ph/9812320]; S. Heinemeyer, W. Hollik and G. Weiglein, *Eur. Phys. J. C* **9** (1999) 343 [arXiv:hep-ph/9812472]; G. Degrossi, S. Heinemeyer, W. Hollik, P. Slavich and G. Weiglein, *Eur. Phys. J. C* **28** (2003) 133 [arXiv:hep-ph/0212020].; M. Frank, T. Hahn, S. Heinemeyer, W. Hollik, H. Rzehak and G. Weiglein, JHEP **0702** (2007) 047 [arXiv:hep-ph/0611326].
- [42] S. Chen *et al.* [CLEO Collaboration], Phys. Rev. Lett. **87** (2001) 251807 [arXiv:hep-ex/0108032]; P. Koppenburg *et al.* [Belle Collaboration], Phys. Rev. Lett. **93** (2004)

- 061803 [arXiv:hep-ex/0403004]. B. Aubert *et al.* [BaBar Collaboration], arXiv:hep-ex/0207076; E. Barberio *et al.* [Heavy Flavor Averaging Group (HFAG)], arXiv:hep-ex/0603003.
- [43] G. Bennett *et al.* [The Muon g-2 Collaboration], *Phys. Rev. Lett.* **92** (2004) 161802, hep-ex/0401008; G. Bennett *et al.* [The Muon g-2 Collaboration], *Phys. Rev. D* **73** (2006) 072003 [arXiv:hep-ex/0602035].
- [44] T. Falk, K. A. Olive and M. Srednicki, *Phys. Lett. B* **339**, 248 (1994) [arXiv:hep-ph/9409270]; C. Arina and N. Fornengo, *JHEP* **0711**, 029 (2007) [arXiv:0709.4477 [hep-ph]].
- [45] J. R. Ellis, T. Falk and K. A. Olive, *Phys. Lett. B* **444**, 367 (1998) [arXiv:hep-ph/9810360]; J. R. Ellis, T. Falk, K. A. Olive and M. Srednicki, *Astropart. Phys.* **13**, 181 (2000) [Erratum-*ibid.* **15**, 413 (2001)] [arXiv:hep-ph/9905481].
- [46] J. R. Ellis, K. A. Olive and Y. Santoso, *JHEP* **0810**, 005 (2008) [arXiv:0807.3736 [hep-ph]].